IMECE2006-15339

ROBUST DESIGN OF RF-MEMS CANTILEVER SWITCHES USING CONTACT PHYSICS MODELING

Mohammed Shalaby
Department of Mechanical Engineering
University of Michigan, Ann Arbor, MI

Zhongde Wang
Ansoft, Corp., San Jose, CA

Linda L.W. Chow
Department of Mechanical
Engineering
University of Michigan, Ann
Arbor, MI

Brian D. Jensen
Department of Mechanical
Engineering
Brigham Young University,
Provo, UT

John L. Volakis
Department of Electrical and
Computer Engineering
Ohio State University,
Columbus, OH

Katsuo Kurabayashi
Department of Mechanical Engineering
University of Michigan, Ann Arbor, MI

Kazuhiro Saitou
Department of Mechanical Engineering
University of Michigan, Ann Arbor, MI

ABSTRACT

This paper presents the design optimization of a RF-MEMS direct contact cantilever switch for minimum actuation voltage and opening time, and maximum power handling capability. The design variables are the length and thickness of the entire cantilever, the widths of the sections of the cantilever, and the dimple size. The actuation voltage is obtained using a 3D structural-electrostatic FEM model, and the opening time is obtained using the same FEM model and the experimental model of adhesion at the contact surfaces developed in our previous work. Since the precise control of the contact resistance during the micro machining process is practically impossible, the power handling capability is estimated as the ratio of the RMS power of the RF current ("signal") passing through the switch to the contact temperature ("noise") resulting from the possible range of the contact resistance. The resulting robust optimization problem is solved using a Strength Pareto Evolutionary Algorithm, to obtain design alternatives exhibiting different trade-offs among the three objectives. The results show that there exists substantial room for improved designs of RF MEMS direct-contact switches.

INTRODUCTION

The introduction of surface micromachining techniques to the conventional microwave integrated circuit processing enabled a new class of radio-frequency switches, RF MEMS (Radio Frequency Micro-Electro-Mechanical-System) direct-contact switches. RF-MEMS direct contact switches possess superior characteristics such as wide band, ultra-low loss, high linearity, and negligible power consumption [1]. Typically, less than 0.1 dB loss from DC to 100 GHz with power consumption on the order of micro-watts is obtained by using high conductivity metallic materials [2], [3]. Such wide band low-loss switches can be used in radar and communications antennas [4]-[6], and tunable filters [7]-[9].

However, they also suffer from several unfavorable drawbacks including high actuation voltage, low power handling capability, and long opening time [10]. The actuation voltage is the DC voltage applied to pull the switch body down to an operational contact state. It is highly related to the geometry and structural properties of the switch body that influence its stiffness. The power handling capability is the maximum allowable RF power that can pass through the switch body without changing the operational contact resistance. It is highly related to the temperature of the contact surfaces. For switches made of sputtered gold, the temperature should be maintained between 60 and 80°C, since the lower temperature causes the unbounded increase in the contact resistance [11] and the higher temperature causes the melting and welding of the contact surfaces. The opening time is the time between the turning off of the actuation voltage and the physical separation of the two contact surfaces. It is highly related to the size of the contact dimple that influences the adhesion force between the contact surfaces.

This paper presents the design optimization of a RF-MEMS direct contact cantilever switch (Figure 1) for minimum actuation voltage and opening time, and maximum power handling capability. The design variables are the length and

thickness of the entire cantilever, the widths of the sections of the cantilever, and the dimple size. The objectives are the actuation voltage, the switch opening time, and the power handling capability. FEM combined with an experimental model of adhesion at the contact surfaces [12] are used to evaluate these objectives. Due to the difficulty in precisely controlling contact resistance during the micro machining process, the power handling capability is estimated using the signal-to-noise ratio model [13],[14], where the signal is the ratio of the RMS power of the RF current passing through the switch and the noise is the contact temperature resulting from the possible range of the contact resistance. The resulting robust optimization problem is solved using a Strength Pareto Evolutionary Algorithm (SPEA) [15],[16], in order to obtain Pareto-optimal design alternatives exhibiting different trade-offs among the three objectives.
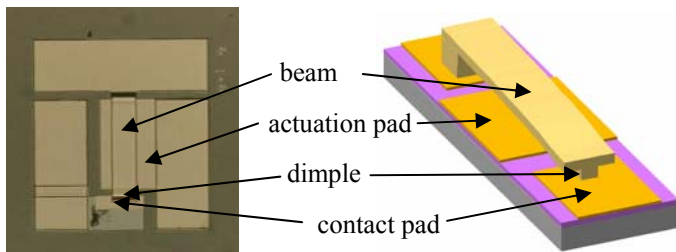

Figure 1: RF MEMS direct contact cantilever switch

RELATED WORK

Characterization and modeling of RF-MEMS switches

A number of researchers have studied the performance of RF MEMS switches and pointed out some unfavorable drawbacks. Chan *et al* [17] and Goldsmith *et al.* [18] indicated that a high actuation voltage may lead to a shorter lifetime for direct contact and capacitive MEMS switches. Schauwecker *et al.* [19], and Rebeiz and Muldavin [20] point out that that the power handling capability should be lower than 100 mW whereas most wireless applications require 1~2 W.

Electromagnetic modeling of RF MEMS switches is a challenging task due to the tiny electrical dimensions and the switch motion during the operation [21]. Few papers suggest solutions to these challenges, such as Finite Difference Time Domain (FDTD) [22] and Moment Method [1], [23]. Wang *et al.* [21] developed an extended finite-element boundary-integral (EFE-BI) method by applying a conventional FE-BI [23] on the substrate and a BI for the switch beam. Chow *et al.* [24] used air-suspended transmission lines to experimentally validate this full-wave EM model [21] integrated with a thermal model. They also developed a closed-form thermal model capturing the skin effect. This latter model saves computational time, and demonstrates very reasonable accuracy; therefore, it is adopted in the present study.

Contact modeling for RF-MEMS switches

Understanding the thermal and mechanical behavior of contact surfaces during the switch operation is a key for improving performance, reliability, and power handling capability of the RF MEMS direct contact switches. Greenwood and Williamson developed a classical model of contact heating in 1958 based on the assumption that equipotential surfaces are coincident with the isotherms in the contact [25]. In our previous work, Jensen *et al.* [12] extended the model and further demonstrated the control of the contact resistance by a softening temperature. When the contact temperature exceeds the contact material softening temperature the contact resistance drops drastically and remains low.

Switch opening time reduces with contact adhesion. Most of the existing models and experiments in MEMS adhesion are concerned with steady-state behavior. Jensen *et al.* developed a kinetic model of switch opening time based on bond dissociation [11], which is adopted in the present study.

Optimization of RF-MEMS switch

Ducarouge *et al.* [26] developed a design method for fixed-fixed RF-MEMS switches. The method optimized the beam geometry by varying only 3 width variables. Miao *et al.* [27] controlled the performance of a capacitive fixed-fixed RF-MEMS switch by changing the geometry at both ends of the beam to have smaller width, thus reduce the switch stiffness. On the other hand, Huang *et al.* [28] divided the beam into several sections, each with a different width and length defined for each to have more control on the switch performance. Artificial Neural Network (ANN) was used to simulate the full wave electromagnetic model but in less time [29]. The input variables were the beam length and width, while the insertion and return loss were the output variables.

None of the above models dealt with cantilever RF-MEMS switches even though they have better structural properties and are less prone to buckling. In addition, these models only handled one or two of the common RF-MEMS switch drawbacks. Finally, they considered only few design variables.

Robust design optimization

Taguchi [13] defined robustness as the insensitivities of the system performance to the parameters that are uncontrollable by the designer. Since any systems operating in the real world are under influence of the operating environment that are beyond the full control of the designer, it is widely accepted as a criterion for improving and optimizing products and systems. Robust design optimization incorporates this concept of robustness into design optimization and aims at achieving the designs that optimize given performance measures as well as minimizing the sensitivities against uncontrollable parameters using different approaches, such as the signal to noise ratio [30]-[32].

Since contact resistance, a key system parameter affecting power handling of RF MEMS switches, is virtually impossible to be precisely controlled during the micro machining process,

the present study adopts robust design optimization, where the contact resistance is regarded as an uncontrollable parameter.

ROBUST OPTIMIZATION OF RF MEMS SWITCHES

Overview

The robust optimization problem of RF MEMS direct contact cantilever switches studied in this paper is summarized as follows:

- **Given:** switch material properties (mechanical, electrical and thermal including), parametric geometry of cantilever beam and contact dimple, height of contact dimple, gap length between switch beam and substrate, and possible range of contact resistance
- **Find:** dimensions of beam and dimples, and RF current
- **Subject to:** realization of a feasible contact temperature regardless variation in contact resistance
- **Minimizing:** actuation voltage, switch opening time
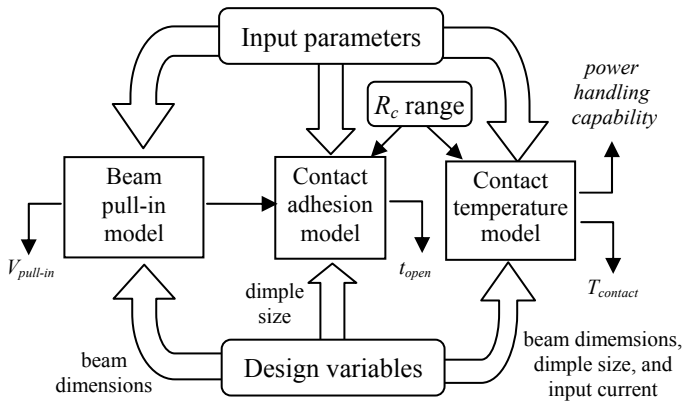- **Maximizing:** power handling capability of switch

Figure 2: Inputs and outputs of models

The optimization problem is solved using a Strength Pareto Evolutionary Algorithm to obtain Pareto-optimal design alternatives exhibiting different trade-offs among the three objectives: the actuation voltage, the switch opening time, and the power handling capability.

Figure 2 shows the input-output relationship of the mathematical models to compute the three objectives. The actuation voltage ($V_{pull-in}$) is obtained using a 3D structural-electrostatic FE model of beam pull-in, based on the beam geometry. The switch opening time (t_{open}) is obtained using the experimental model of adhesion at the contact surfaces developed in our previous work [11], based on the dimple size, and possible range of contact resistance, and the restoring force ($F_{restore}$) of the beam at down state without the actuation voltage. The power handling capability is obtained using an analytical model of the contact temperature integrated with a 2D thermal FE model of the entire beam. It is estimated as the ratio of the RMS power of the RF current passing through the

switch ("signal") to the contact temperature ("noise") resulting from the possible range of the contact resistance, based on beam geometry, dimple size, input RF current to the switch, and the possible range of contact resistance.

Structural/electrostatic model

Figure 3 shows a cross section of a cantilever switch along its length (*x*-axis). When actuation voltage is applied to the actuation pad, electrostatic field at the gap between the beam and the pad creates a downward electrostatic force $q(x)$ along the beam length, which in turn causes the vertical displacement of beam $w(x)$. For given actuation voltage V, electrostatic force $q(x)$ can be approximated by a micro-strip line model similar to a capacitive model as shown in equations (1)-(5) [33]:

$$q = \frac{1}{2}V^2 \frac{\partial c(w)}{\partial w} = \frac{1}{2}V^2 \frac{c(w+\Delta w) - c(w-\Delta w)}{2\Delta w} \quad (1)$$

$$c = \frac{1}{Z_c \sqrt{\mu_0 \varepsilon_0}} \quad (2)$$

$$Z_c = \frac{1}{2\pi}\sqrt{\frac{\mu_0}{\varepsilon_0}} \ln\left[F_1 \frac{g_t + w}{b_e} + \sqrt{1 + \left(2\frac{g_t + w}{b_e}\right)^2} \right] \quad (3)$$

$$F_1 = 6 + (2\pi - 6)\exp\left\{-\left[30.666(g_t + w)/b_e\right]^{0.7528}\right\} \quad (4)$$

$$b_e = b + \frac{t}{\pi}\left\{1 + \ln\left[2\frac{g_t + w}{t}\right]\right\} \quad (5)$$

where b is the beam width, t is the beam thickness, g_t is the total initial gap, b_e is the effective beam width, F_1 is a numerical parameter with no physical significance, μ_0 is the permeability of free space ($=4\pi$x10^{-7} H/m), ε_0 is the permittivity of free space ($=8.85$x10^{-12} F/m), Z_c is the characteristic impedance of the equivalent microstrip line, and $\Delta w = 1$ nm.
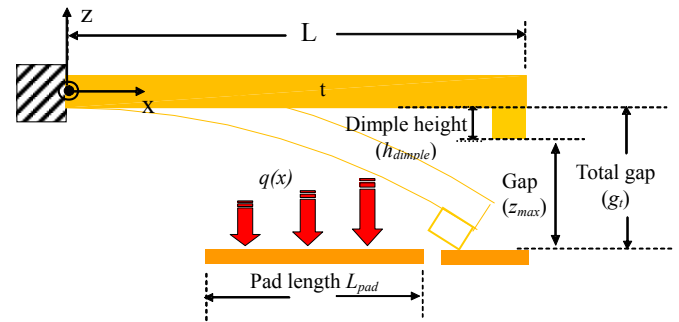

Figure 3: Cross section along the length switch showing the structural model

The minimum voltage that can put the switch in this state is called the actuation voltage ($V_{pull-in}$). In this case the switch is barely touching the contact pad, which makes the reaction force to the dimple equal to zero. It is obvious, as a result, that the reaction force at the dimple is proportional (though not linearly

proportional) to the applied voltage. If the applied voltage is too small, the reaction force is negative, meaning that extra force is needed at the dimple to pull the switch to the operational state. Similarly, when the applied voltage is high enough, the reaction force is positive, meaning that the switch is applying force on the contact pad.

Based on this reasoning, the actuation voltage that gives zero reaction force to the dimple is iteratively as follows.

1. Apply the initial (artificial) displacement at the beam, such that the dimple touches the contact pad. Set actuation voltage $V = V_0$ (initial guess).
2. Calculate vertical displacement $w(x)$ using the structural model
3. Calculate electrostatic force $q(x)$ for $w(x)$ and V using the electrostatic model.
4. If reaction force at the dimple $F_{react} < 0$, increase V. If $F_{react} > 0$, decrease V. Otherwise return V.
5. Go to 2.

In our implementation, a combination of bisection, secant, and inverse quadratic interpolation methods [34], [35] is used to find the next iterate of V at step 4.

In addition to $V_{pull-in}$, the restoring force ($F_{restore}$) necessary for the switch opening time can be obtained by calculating F_{react} with zero actuation voltage.

Table 1 shows a comparison of our method with the commercial code CoventorWare for the reaction force (F_r) at the fixed support and at the dimple (contact force, F_c) with different applied voltages (for a switch with L= 200 μm, W=20 μm, t=2 μm, g=2 μm, L_{pad} =160 μm, material gold with E=78 GPa, v=0.44). The results agree quite well.

Table 1: Comparison of our model with CoventorWare (CW)

Applied Voltage (V)		4	8	10	12	16	20	24
F_r (μN)	CW	0.073	0.320	0.794	0.983	1.463	2.135	3.083
	Our model	0.072	0.313	0.794	0.976	1.438	2.075	2.985
F_c (μN)	CW	N/A	N/A	N/A	0.084	0.506	1.097	1.960
	Our model	N/A	N/A	N/A[1]	0.085	0.505	1.098	1.949

Contact adhesion model

Assuming gold as contact material, modeling of contact opening time uses chemical kinetics to derive a differential equation for the number of gold-gold bonds in the contact area [11]:

$$\frac{\partial N_2}{\partial ti} = -N_2 k_{02} \exp\left[\frac{K_2 F_{restore} x_2}{k_B T (\phi_1 A_a + K_2 N_2)}\right] \tag{6}$$

where, N_2 is the number of gold-gold bonds, ti is time, k_{02} is the bond dissociation rate constant, K_2 is the gold bond stiffness, $F_{restore}$ is the restoring force acting to open the contact, x_2 is a numerical parameter roughly equivalent to the distance a gold-

---

[1] **The applied voltage less than the pull-in voltage**

gold bond can stretch before breaking, k_B is the Boltmann constant, T is the temperature, ϕ_1 is a numerical parameter describing the density and stiffness of any bonds other than gold-gold bonds in the contact area, and A_a is the apparent contact area, typically the area of the contact dimple in a switch. Switch opening time t_{open} is time at which all gold-gold bonds dissociate between the contact surfaces, *i.e.*, $N_2 = 0$.

Equation (6) is solved numerically using the initial condition

$$N_{2_0} = \rho_2 (\pi a^2) \tag{7}$$

where ρ_2 is the area density of gold-gold bonds and a is the radius of the real contact spot, or the spot where real gold-gold contact takes place. The theoretical contact resistance value is related to a by [36]:

$$R_c = \frac{4 \rho_e \lambda}{3 \pi a^2} + \left[\frac{1 + 0.83 (\lambda/a)}{1 + 1.33 (\lambda/a)}\right] \frac{\rho_e}{2a} \tag{8}$$

where R_c is the contact resistance, ρ_e is the electrical resistivity in the metal (assumed to be the same for both contact surfaces), and λ is the mean free path of an electron. In reality, the contact resistance is not deterministic, due to manufacturing inaccuracies.

The solution of (6) depends on restoring force $F_{restore}$ obtained by the beam pull-in model, the apparent contact area A_a calculated with the dimple dimensions, and the contact resistance R_c which is taken as the median (1.5 Ω) of its possible range (1.3-1.7 Ω). Other parameters values are available through either measurements or in the literature [21]. However, the three parameters, k_{02}, x_2, and ϕ_1, were found by fitting the model predictions to experimental data [11]. The values of all the parameters used in this paper are summarized in Table 2.

Table 2: Values of parameters used in modeling contact opening time [11]

Parameter	Value	Unit
k_{02}	3.52x10^{-3}	ms^{-1}
x_2	0.021	Nm
ϕ_1	12,320	μN/μm^3
K_2	12	N/m
ρ_2	12x10^6	Bonds/μm^2
λ	38	Nm
ρ_e	3.6x10^{-6}	Ω-m

Contact temperature model

When RF current passes through the switch, Joule heating causes temperature rise, especially at the contact surfaces, where the electric resistance is higher than the one of the switch body. This localized temperature rise at the contact surfaces is the major limiting factor of the power handling capability of RF-MEMS switches. For switches made of sputtered gold, the temperature should be maintained between

60 and 80˚, since the lower temperature causes the unbounded increase in the contact resistance [12] and the higher temperature causes the melting and welding of the contact surfaces.

Current flow in the switch causes Joule heating according to the heat transfer equation:

$$-\kappa \nabla^2 T = P_d = J^2 \rho \qquad (9)$$

where κ is the thermal conductivity, T is the temperature, P_d is the dissipated electrical power, J is the current density induced by the input RF power, and ρ is the electrical resistivity of the material. The temperature varies negligibly across the thickness of the beam compared with the beam length and width, so that 2-D finite element modeling is used. Since the electrical signal period (1/radio frequency) is sufficiently smaller than the thermal response time so that the electrical dissipation appears constant for heat transfer, the root mean square (rms) value of the current density can be used for J.

The additional heat generated at the contact due to the contact resistance R_c is simply added to the heat generation of the finite elements on the contact surfaces. This heat is approximated as $I_0^2 R_c / 2$, where I_0 is the rms RF current. Since the power handling capability is directly proportional to I_0^2, one can simply maximize I_0 to maximize the RF power input that a switch can handle. Accordingly, rms RF current I_0 is regarded as one of the design variables, and its power, not the RF power input, is regarded as one of the design objectives to be maximized, as detailed in the following section.

The thermal conduction under the switch body through the air in the gap, g_c, between the switch body and the substrate is modeled using a thermal resistance, R_{th1}, placed between each beam element and the gold contact pad on a silicon substrate, and is assumed to remain at ambient temperature. The thermal resistance is given as

$$R_{th1} = \frac{g_c}{\kappa_a A} \qquad (10)$$

The thermal contact resistance under the contact dimple accounts for thermal conduction through the air surrounding the metal contact spots on the contact dimples, Equation (10), and through metal contact spots:

$$R_{th2} = \frac{R_c}{\rho \kappa_m} . \qquad (11)$$

where R_c is the contact resistance; κ_a and κ_m are the air and metal thermal conductivity respectively.

The local asperity temperature is expected to be higher than the bulk contact temperature given by Equations (9)-(11), because current flow heats the contact [37], [38]. Taking into account the high-frequency effect [39], contact temperature can be approximated by [25]:

$$T_{contact} = \sqrt{\frac{\alpha V^2}{4L} + \frac{T_2^2 + T_0^2}{2}} - T_0 \qquad (12)$$

where, T_2 is the average temperature over the dimple given by Equations (9)-(11), T_0 is the ambient temperature on the substrate, L is the Lorentz constant (2.45 x 10^{-8} V^2/K^2), $V=I_0 R_c$ is the voltage drop over the contact region, R_c is the contact resistance, $\alpha = \gamma R_m / R_c$, $R_m = \rho / 2a$ ($\mu\Omega$), a is the radius of the contact spot, $\gamma = (1 + 0.83\lambda/a)/(1 + 1.33\lambda/a)$, ρ is the gold conductivity (3.58 x $10^{-8}\Omega$– m).

Equation (12) shows that the contact temperature is mainly dependent on the electrical contact resistance (typically between 1~2 Ω), rms of RF current, and the dimple size, as the dimple size affects the thermal contact resistance. On the other hand, the beam shape and dimensions have negligible effect on the contact temperature. Our previous work [40] indeed confirmed that the increased dimple size decreases the thermal resistance, and in turn decreases contact temperature, and vice versa. Since contact temperature $T_{contact}$ in Equation (12) has to lie in the 60~80 ˚C range, only a specific range of rms of RF current and dimple size are feasible.

Definition of design variables

There are fifteen (15) design variables as follows:

- $y_1, ..., y_{10}$: widths of the beam at equally spaced sections along the beam length
- L, t: length and thickness of the beam
- d_l, d_w: length and width of the dimple
- I_0: rms RF current

Figure 4s (a) and (b) show the top and side views of the switch, respectively, with all the dimensions design variables. As shown in Figure 4, the beam is assumed to be symmetric with respect to its longitudinal axis, and the length and location of the actuation pad determined relative to the beam length L; the actuation pad always starts at $L/10$ and ends at $8L/10$ from the anchor.
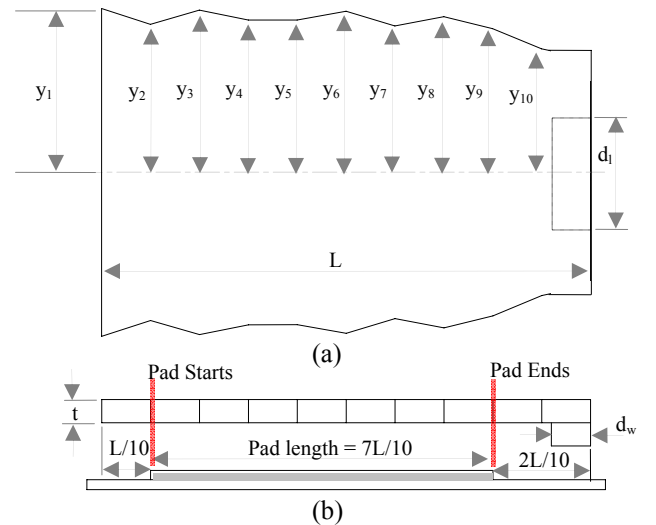

(a)

(b)

Figure 4: Switch geometry and design variables

Definition of design objectives

We aim at RF-MEMS switch designs with low pull-in voltage $V_{pull\text{-}in}$, short opening time t_{open}, and high power handling capability or equivalently the square of rms RF current I_0. While I_0 is also a design variable, it is upper bounded since contact temperature $T_{contact}$ depends on I_0 as shown in Equation (12) and $T_{contact}$ must lie between 60 and 80 ^{o}C. However, values of t_{open} and I_0^2 cannot be used, as they are, as objectives for optimization since they depend on contact resistance R_c, a uncontrollable variable that may take any values within the given possible range (1.3-1.7 Ω). To achieve an optimum design that is insensitive to the variation of R_c, the design objectives associated with t_{open} and I_0^2 are formulated using the signal to noise ratio method [13], [30].

In the case of opening time, the signal is the value of t_{open} at R_c = 1.5 Ω, the median of the possible range, and the noise is the difference between the maximum and minimum values of t_{open} due to the variation in R_c. In the case of the power handling capability, the signal is the value of I_0^2, and the noise is the difference between the maximum and minimum values of I_0^2 $T_{contact}$ due to the variation in R_c. The "noise" of I_0^2 is taken as the variation of $T_{contact}$ since I_0^2 does not depend on R_c and the variation of $T_{contact}$, which depends on I_0 and R_c, needs to be minimized. The results of the monotonicity analysis for t_{open} and $T_{contact}$ show that they vary monotonically with respect to R_c. Accordingly, the maximum (1.7) and minimum (1.3) values of R_c are used to obtain noise in the opening time and the noise contact temperature (Δt_{open} and ΔT). In summary, the objective functions can be written as:

- To be minimized: f_1, f_2
- To be maximized: f_3

where

$$f_1 = V_{pull\text{-}in} = V\left(y_1,,\cdots,y_{10},L,t\right) \tag{13}$$

$$f_2 = t_{open @ R_c =1.5} \times \Delta t_{open} \tag{14}$$

$$f_3 = \frac{I_0^2}{\Delta T} \tag{15}$$

$$\Delta t_{open} = t_{open @ R_c =1.3} - t_{open @ R_c =1.7} \tag{16}$$

$$\Delta T_{contact} = T_{contact @ R_c =1.7} - T_{contact @ R_c =1.3} \tag{17}$$

Definition of constraints

The upper and lower bounds of the beam widths, length and thickness are obtained based on the micromachining capabilities available. The lower bound on d_w and d_l is set to be equal to 1.1 μm, the skin depth at a typical operational frequency of 5 GHz to confine all RF energy without any radiation. The pull in voltage is constrained not to exceed 80V, and the opening time has an upper bound of 100 μs, which are the practical values. Finally, the contact temperature has to stay between 60-80°C regardless of the contact resistance value. In summary, the constraints can be written as:

$$10 \le y_1,\cdots,y_{10} \le 75 \mu m \tag{18}$$

$$200 \le L \le 400 \mu m \tag{19}$$

$$0.5 \le t \le 5 \mu m \tag{20}$$

$$0.11 \le d_l, d_w \le 10 \mu m \tag{21}$$

$$10 \le I_0 \le 1000 mA \tag{22}$$

$$V_{pull\text{-}in} \le 80V \tag{23}$$

$$t_{open} \le 100 \mu s \tag{24}$$

$$60 \le T_{@ R_c =1.3}, T_{@ R_c =1.7} \le 80 ^o C \tag{25}$$

Optimization algorithm

Since the above optimization problem is multi-objective, Strength Pareto Evolutionary Algorithm (SPEA) [15], [16] is used to find the trade off among the conflicting design objectives. SPEA has several advantageous characteristics over the conventional multi-objective genetic algorithm, namely a) the non-dominated solutions are sorted externally in a second, continuously updated population, b) the individual's fitness is evaluated with respect to the number of external non-dominated points that dominate it, c) the Pareto dominance relationship preserves the population diversity, and d) a clustering procedure is used to reduce the non-dominated set without destroying its characteristics [15]. Side constraints (18)-(22) are embedded in the chromosome encoding of the algorithm, while constraints (23)-(25) are handled as penalties to respective objective functions. The parameters used in the SPEA are summarized in table 3.

Table 3: Parameters for SPEA

Parameter	Value
Population size	100
Number of generations	120
External population size	50
Crossover probability	0.50
Mutation probability	0.15

RESULTS AND DISCUSSION

The resulting Pareto optimal solutions in the objective function space are shown in Figures 5 and 6. Figure 5 shows it in the 3D objective function space, while Figures 6 (a), (b), and (c) show its 2D projections with respect to objective 1 and 2, 1 and 3, and 2 and 3, respectively.

All Pareto optimal solutions have almost the same values for beam length ($L = 200$ μm), beam thickness ($t = 5$ μm), dimple width ($d_w = 1.1$ μm), and rms RF current ($I_0 = 53.5$ mA). As the beam thickness increases, the switch stiffness increases; consequently, the switch opening time descreases. This can be a reason why the thickness reached the upper bound in all the given results. The optimizer also tries to maximize the beam width at the actuation pad, this way the area affected by the voltage is maximized and so the pull in force can be maximized to the same voltage value. The opening time is affected by the width of the beam near the anchoring point; when the beam width at the anchoring point increases,

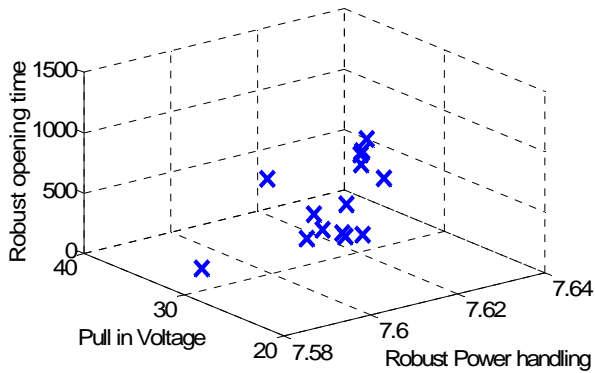the pull in voltage increases and the opening time decreases, and vice versa.

Figure 5: Pareto Solution in 3D objective function space

The two most promising results denoted as 1 and 8 in Figures 5 and 6, are shown in Figures 7 and 8. The red lines represent the lines connecting the optimized coordinates of the beam (*i.e.,* beam geometry). The figures show only half of the beam as the other half is symmetric. Figure 7 shows the design with minimum opening time because it has maximum stiffness, owing to its wide cross section at the anchoring point. The voltage required to pull the switch in is also large to induce the large amount of force needed to overcome the switch stiffness. On the other hand, Figure 8 shows the design with longer opening time, 3 times longer. The switch cross section at the anchoring point is slightly less than half the cross section of the previous solution. Since the stiffness of the switch is lower, the voltage required to pull the switch in is much less. Both designs do not have any sharp edges that may cause undesired stress concentration and can be easily manufactured.

The remaining twelve Pareto optimum results that have practical opening time and pull in voltage results (<50 µs and < 35 V, respectively) are shown in appendix A. Although experimental validation is yet to be seen, these results suggest that there is a substantial room for optimized RF-MEMS switches to achieve better performance than the typical values reported in the literature: opening time of 50µs-200ms, pull-in voltage of 50-80V, and power handling of 20-50mW [20].

CONCLUSION

This paper presented an integrated multi-physics model of RF-MEMS cantilever direct contact switches, and the optimization of switch geometry using the model. The objectives were to minimize pull-in voltage and opening time, and to maximize power handling capability. The problem was formulated as multi-objective robust optimization such that the switch performances are insensitive to the variations of the contact resistance that cannot be precisely controlled during micromachining process. A multi objective genetic algorithm, SPEA, was used to obtain the Pareto optimum solutions that exhibit different trade offs among the three objectives.

The results provided the better understanding of key factors contributing to the performances of RF-MEMS switches, and the guides and insights for further improvements of RF-MEMS switches that exploits complex multi-physics phenomena.
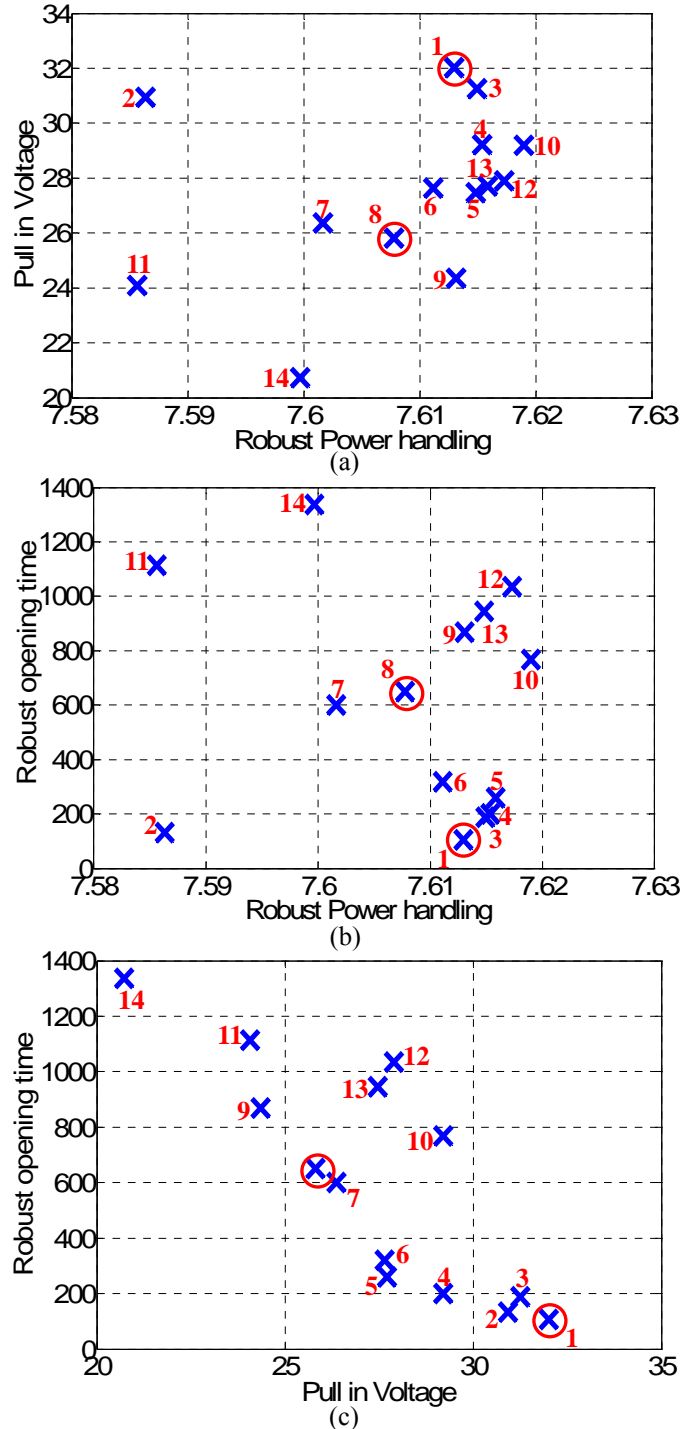

Figure 6: Pareto Solution projected in 2D. (a) power handling vs. pull-in voltage, (b) power handling vs. opening time, and (c) pull-in voltage vs. opening time
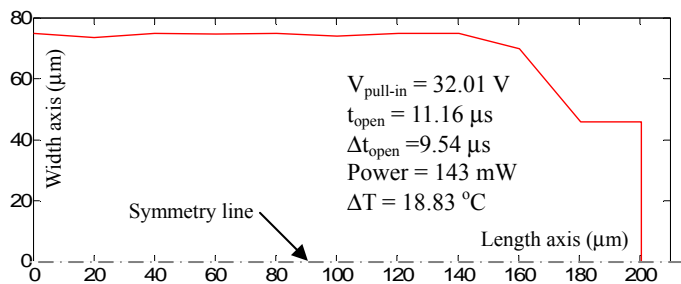
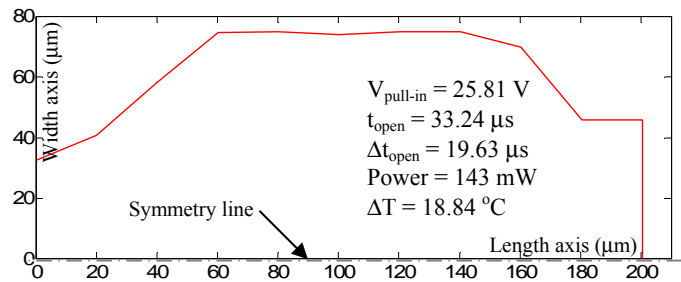**Figure 7: Switch geometry (half shown) for minimum opening time (Pareto point 1)**

$V_{pull\text{-}in}$ = 32.01 V
t_{open} = 11.16 μs
Δt_{open} = 9.54 μs
Power = 143 mW
ΔT = 18.83 ^{o}C

Figure 8: Switch geometry (half shown) for low pull-in voltage (Pareto point 8)

$V_{pull\text{-}in}$ = 25.81 V
t_{open} = 33.24 μs
Δt_{open} = 19.63 μs
Power = 143 mW
ΔT = 18.84 ^{o}C

REFERENCES

[1] Rebeiz, G., 2002, *RF MEMS- Theory, Design, and Technology*, Wiley, New Jersey.

[2] Goldsmith, C., Yao, Z., Eshelman, S. and Denniston, D., 1998, "Performance of low-loss RF EMMS capacitive siwthces," IEEE Microwave and Guided Wave Letters, **8**, pp. 269-271.

[3] D. Mercier, P.L. Charvet, P. Berruyer, C. Zanchi, L. Lapierre, O. Vendier, J.L. Cazaux, and P. Blondy, "A DC to 100 GHz high performance ohmic shunt switch, "in *IEEE MTT-S International Microwave Symposium Digest*, 2004, Vol.3, pt. 3, pp. 1931-4.

[4] Norvell, B., Hancock, R., Smith, J., Pugh, M., Theis, S. and Kviatkofsky, J., 1999, "Micro electro mechanical switch (MEMS) technology applied to electronically scanned arrays for space based radar," *Proc. 1999 Aerospace Conference*, Snowmass at Aspen, CO, **3**, pp.239-247.

[5] C. W. Jung, M.-J. Lee, G. P. Li, F. De Flaviis, "Reconfigurable scan-beam single-arm spiral antenna integrated with RF-MEMS switches, "*IEEE Transactions on Antennas and Propagation*, v 54, n 2, pp. 455-63, 2006.

[6] R. N. Simons, D. Chun, L.P.B. Katehi, "Polarization reconfigurable patch antenna using microelectromechanical systems (MEMS) actuators," in *IEEE Antennas and Propagation Society International Symposium* 2002, pt. 2, vol.2, pp. 6-9.

[7] Goldmith, C., Malczewski, A., Yao, Z., Chen, S., Ehmke, J. and Hinzel, D., 1999, "RF MEMS Variable Capacitors for Tunable Filters," Int. J. of RF and Microwave CAE, **9**, pp.362-374.

[8] G. K. Fedder, and T. Mukherjee, "Tunable RF and analog circuits using on-chip MEMS passive components," in *IEEE International Solid-State Circuits Conference* 2005, pt. 1, Vol. 1, pp. 390-1.

[9] S. Lee, J.-M. Kim, J.-M. Kim, J. K. Kim, Y. W. Kwon, "Millimeter-wave MEMS tunable low pass filter with reconfigurable series inductors and capacitive shunt switches, " *IEEE Microwave and Wireless Components Letters*, v 15, n 10, pp. 691-693, 2005.

[10] J. DeNatale, "Reconfigurable RF Circuits based on Integrated MEMS Switches," in *IEEE International Solid-State Circuits Conference (ISSCC* 2004), pp. 310-311

[11] B.D. Jensen, L.L.W. Chow, K. Huang, K. Saitou, J.L. Volakis, and K. Kurabayashi, "Effect of Nanoscale on Electrical Transport in RF MEMS Switch Contacts," *J. Microelectromechanical Systems* V. 14, no. 5, pp. 935-946, Oct, 2005.

[12] Jensen, B., Huang, K., Chow, L. and Kurabayashi, K., 2005, "Adhesion Effects on Contact Opening Dynamics in Micro machined Switches," J. Appl. Phys., **97**, pp. 103535-1 - 103535-9.

[13] Taguchi, G., 1987, *Systems of Experimental Design*, Kraus, International, New York.

[14] Tsutsui S. and Ghosh, A., 1997, "Genetic algorithms with a robust solution searching scheme," IEEE Transactions on Evolutionary Computation, **1**, pp. 201–208.

[15] Zitzler, E. and Thiele, L., 1999, "Multiobjective evolutionary algorithms a comparative case study and the strength pareto approach," IEEE Transactions on Evolutionary Computation, **3**, p 257-271.

[16] Coello, C., Veldhuizen, D., Lmont, G., 2002, *Evolutionary Algorithms for Solving Multi-Objective Problems*, Kluwer Academic Publishers, MA.

[17] Chan, R., Lesnick, R., Becher, D. and Feng, M., 2003, "Low-actuation voltage RF MEMS shunt switch with cold switching lifetime of seven billion cycles," J. of Microelectromechanical Systems, **12**, pp.713-719.

[18] Goldsmith, C., Ehmke, J., Malczewski, A., Pillans, B., Eshelman, S., Yao, Z., Brank, J. and Eberly, M., 2001, "Lifetime characterization of capacitive RF MEMS switches," *IEEE MTT-S International Microwave Symposium Digest*, Phoenix, AZ, **3**, pp. 227-230.

[19] Schauwecker, B., Strohm, K., Simon, W., Mehner, J. and Luy, J, 2002, "A new type of high bandwidth RF MEMS Switch-toggle switch," J. of Semiconductor Technology and Science, **2,** pp. 237-245.

[20] Rebeiz G. and Muldavin, J., 2001, "RF MEMS switches and switch circuits," IEEE Microwave Magazine, **2**, pp. 59-71.

[21] Wang, Z., Jensen, B., Chow, L., Volakis, J., Saitou, K., and Kurabayashi, K., 2006, "electromagnetic and thermal modeling for prediction of heat-dissipation-induced RF-MEMS switch Failure," Journal of Micromechanics and Microengineering, **16**, pp. 157-164

[22] Thiel, W., Tornquist, K., Reano R. and Katehi, L., 2002, "A study of thermal effects in RF-MEMS-Switches using a time domain approach," *IEEE MTT-S International Microwave Symposium Digest*, pp. 235-238.

[23] Volakis, J., Chatterjee, A. and Kempel, L., 1998, *Finite Element Method of Electromagnetics*, IEEE Press, New York.

[24] Chow, L., Wang, Z., Jensen, B., Saitou, K., Volakis, J. and Kurabayashi, K., "Skin-Effect Self-Heating in Air-Suspended RF MEMS Transmission-Line Structures," submitted to J. Microelectromechanical Systems.

[25] J.A. Greenwood and J.B.P. Williamson," Electrical conduction in solids I. Theory of temperature-dependent conductors," Proc. Roy. Soc. London, Series A, *Math. Phys. Sci.*, vol. 246, no. 1244, pp. 13-31, 1958.

[26] Ducarouge, B., Dubuc, D., Melle, S., Grenier, K., Mazenq, L., Bary, L. and Plana, R., 2005, "Efficient topology and design methodology for RF MEMS switches," *Proceedings of SPIE, Smart Sensors, Actuators, and MEMS II*, May 5-11, Spain, **5836**, pp. 535-539.

[27] Miao, M., Xiao, Z., Wu, G., Hao, Y. and Zhang, H., 2002, "Capacitive RF MEMS switch with composite beam," *Proceedings of SPIE, MEMS/MOEMS Technologies and Applications*, Oct. 17-18, China, **4928**, pp. 248-255.

[28] Huang, J., Liew, K., Wong, C., Rajendran, S., Tan, M. and Liu, A., 2001, "Mechanical design and optimization of capacitive micromachined switch," Sensors and Actuators A, **93**, pp. 273-285.

[29] Lee, Y. and Filipovic, D., 2005, "ANN based electromagnetic models for the design of RF MEMS switches," IEEE Microwave and Wireless Components Letters, **15**, pp. 823-825.

[30] Madu, I. and Madu, C., 1999, "Design optimization using signal-to-noise ratio," Simulation Practice and Theory, **7**, p 349-372.

[31] Fowlkes W. and Clyde M., 1995, *Engineering Methods for Robust Product Design*, Addison-Wesley, MA.

[32] Ramakrishnan, B., and Rao, S. , 1991, "A Robust Optimization Approach Using Taguchi's Loss Function for Solving Nonlinear Optimization Problems," ASME Design Engineering Division, Advances in Design Automation, **32**, p 241-248

[33] Gardiol, F., 1994, *Microstrip Circuits*, Wiley, New York.

[34] MATLAB R14 V7.1, ©1984-2005, The MathWorks, Inc, www.mathworks.com

[35] Forsythe, G., Malcolm, M. and Moler, C., 1976, *Computer Methods for Mathematical Computations*, Prentice-Hall.

[36] Nikolic´, B. and Allen, P., 1999, "Electron transport through a circular constriction," Physics. Review B, **60**, pp. 3963–3969.

[37] Timsit, R., 1999, "Electrical contact resistance: Properties of stationary interfaces," IEEE Trans. on Components and Packaging Technology, **22**, pp.85-98.

[38] Holm, R., 1976, *Electrical contacts, Theory and Applications*, Berlin, Germany, Spring-Verlag.

[39] Jensen, B., Huang, K., Chow, L. and Kurabayashi, K., 2005, "Low-force contact heating and softening using micromechanical switches in diffusive-ballistic electron transport transition," Applied Physics Letters, **86**, pp. 023507-1 - 023507-3.

[40] Wang, Z., Jensen, B., Chow, L., Volakis, J., Saitou, K., and Kurabayashi, K., 2004, "Effects of Dimple Geometry on RF MEMS Switch heating," *Proc. 10th International Symposium on Antenna Technology and Applied Electromagnetics*, Ottawa, Canada.
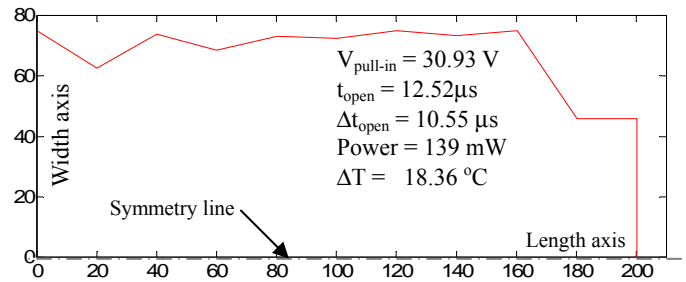
APPENDIX A

$V_{pull-in}$ = 30.93 V
t_{open} = 12.52μs
Δt_{open} = 10.55 μs
Power = 139 mW
ΔT = 18.36 °C

Figure A1: Switch geometry for Pareto Point 2

$V_{pull-in}$ = 31.26 V
t_{open} = 15.31 μs
Δt_{open} = 12.34 μs
Power = 143 mW
ΔT = 18. 79 °C
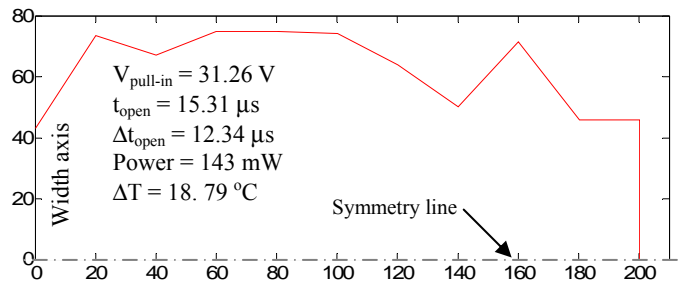
Figure A2: Switch geometry for Pareto Point 3

$V_{pull-in}$ = 29.21 V
t_{open} = 15.87 μs
Δt_{open} = 12.65 μs
Power = 143 mW
ΔT = 18.79 °C
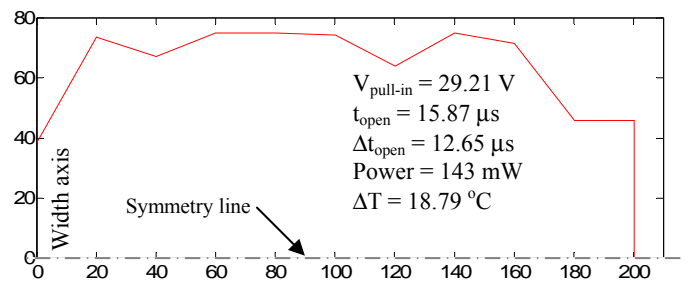
Figure A3: Switch geometry for Pareto Point 4

$V_{pull-in}$ = 27.71 V
t_{open} = 18.50 μs
Δt_{open} = 14.07 μs
Power = 143 mW
ΔT = 18.97 °C
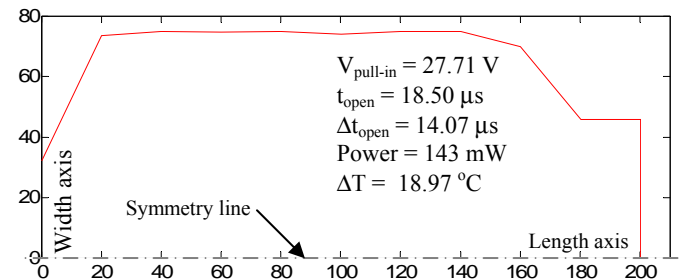
Figure A4: Switch geometry for Pareto Point 5

$V_{pull-in}$ = 27.65 V
t_{open} = 21.31 μs
Δt_{open} = 14.97 μs
Power = 143 mW
ΔT = 18.83 °C

Width axis
Symmetry line
Length axis
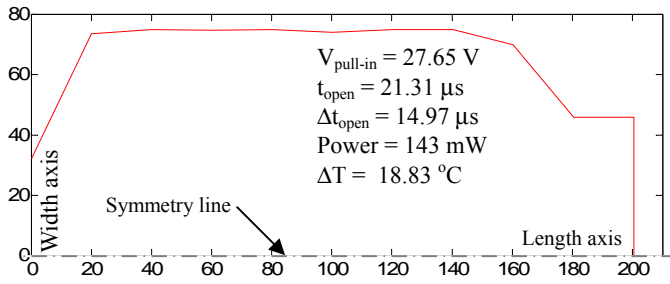
Figure A5: Switch geometry for Pareto Point 6

$V_{pull-in}$ = 26.37 V
t_{open} = 30.85 μs
Δt_{open} = 19.49 μs
Power = 142 mW
ΔT = 18.63 °C

Width axis
Symmetry line
Length axis
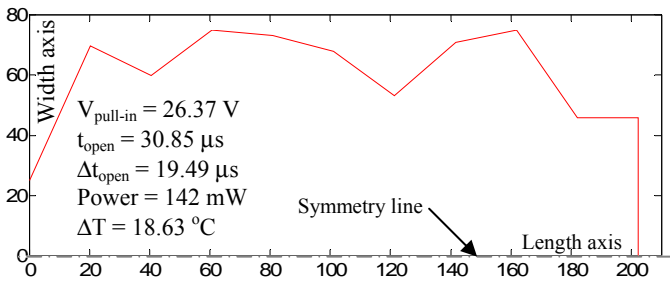
Figure A6: Switch geometry for Pareto Point 7

$V_{pull-in}$ = 24.36 V
t_{open} = 38.43 μs
Δt_{open} = 22.61 μs
Power = 143 mW
ΔT = 18.80 °C

Width axis
Symmetry line
Length axis
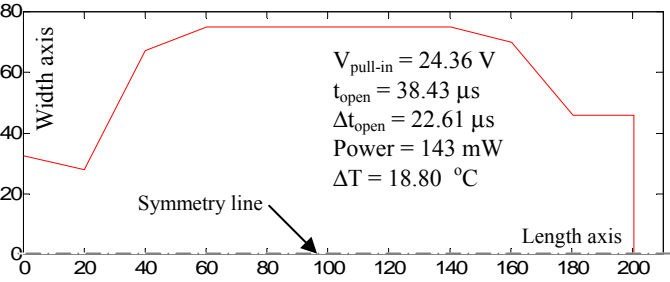
Figure A7: Switch geometry for Pareto Point 9

$V_{pull-in}$ = 29.21 V
t_{open} = 42.81 μs
Δt_{open} = 17.90 μs
Power = 145 mW
ΔT = 19.07 °C

Width axis
Symmetry line
Length axis
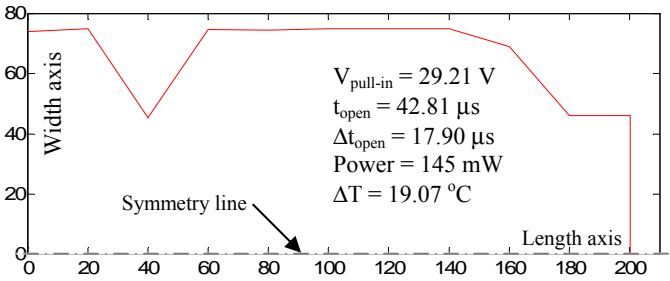
Figure A8: Switch geometry for Pareto Point 10

$V_{pull-in}$ = 24.08 V
t_{open} = 45.26 μs
Δt_{open} = 24.26 μs
Power = 140 mW
ΔT = 18.46 °C

Width axis
Symmetry line
Length axis
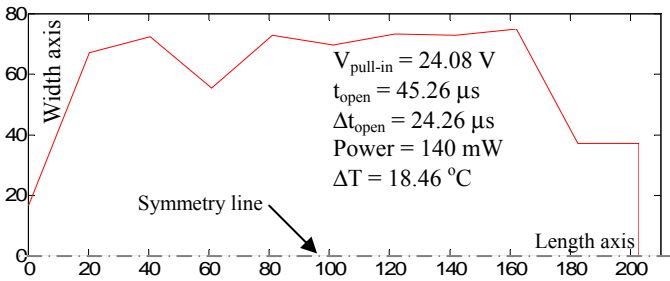
Figure A9: Switch geometry for Pareto Point 11

$V_{pull-in}$ = 27.89 V
t_{open} = 48.89 μs
Δt_{open} = 21.16 μs
Power = 145 mW
ΔT = 19.07 °C

Width axis
Symmetry line
Length axis
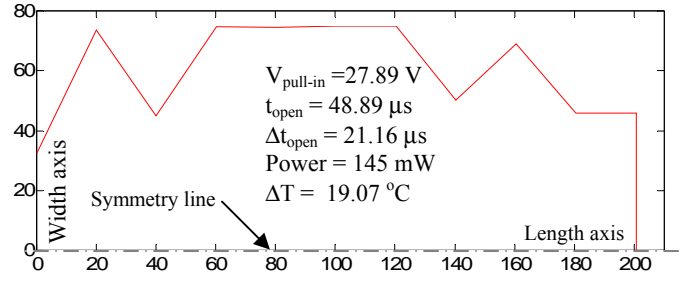
Figure A10: Switch geometry for Pareto Point 12

$V_{pull-in}$ = 27.46 V
t_{open} = 49.00 μs
Δt_{open} = 19.30 μs
Power = 145 mW
ΔT = 19.00 °C

Width axis
Symmetry line
Length axis

Figure A11: Switch geometry for Pareto Point 13

$V_{pull-in}$ = 20.73 V
t_{open} = 49.17 μs
Δt_{open} = 27.19 μs
Power = 140 mW
ΔT = 18.39 °C

Width axis
Symmetry line
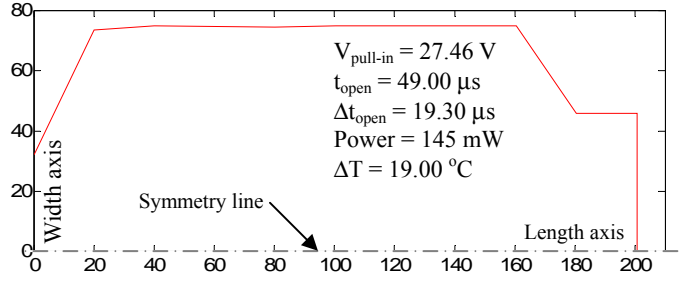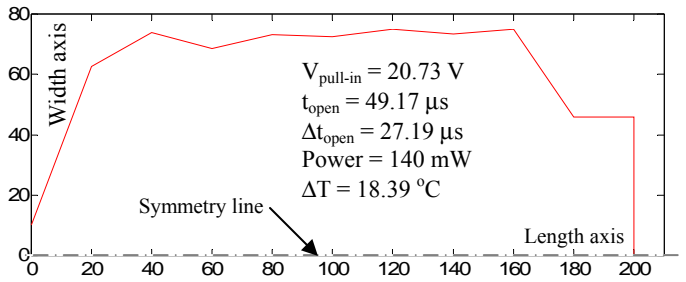Length axis

Figure A12: Switch geometry for Pareto Point 14

10